Article

Geminate Rebinding in R-State Hemoglobin: Kinetic and Computational Evidence for Multiple Hydrophobic Pockets

Silvia Sottini, Stefania Abbruzzetti, Francesca Spyrakis, Stefano Bettati, Luca Ronda, Andrea Mozzarelli, and Cristiano Viappiani

J. Am. Chem. Soc., **2005**, 127 (49), 17427-17432• DOI: 10.1021/ja056101k • Publication Date (Web): 17 November 2005

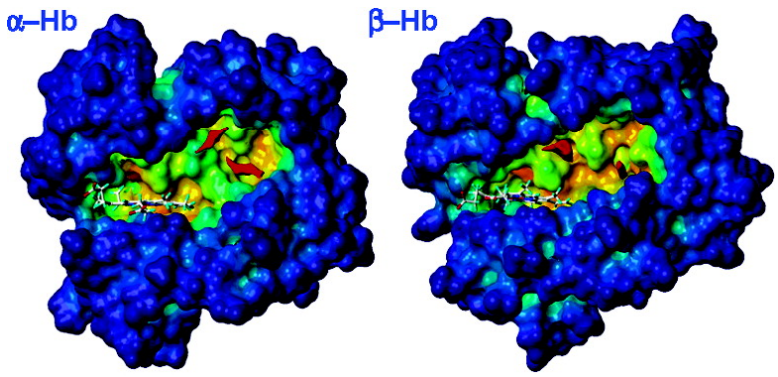

More About This Article

Additional resources and features associated with this article are available within the HTML version:

- Supporting Information
- Links to the 4 articles that cite this article, as of the time of this article download
- Access to high resolution figures
- Links to articles and content related to this article
- Copyright permission to reproduce figures and/or text from this article

View the Full Text HTML

J|A|C|S
ARTICLES
Published on Web 11/17/2005

Geminate Rebinding in R-State Hemoglobin: Kinetic and Computational Evidence for Multiple Hydrophobic Pockets

Silvia Sottini,[†] Stefania Abbruzzetti,[†,||] Francesca Spyrakis,[‡] Stefano Bettati,[§,||] Luca Ronda,[‡,||] Andrea Mozzarelli,[‡,||] and Cristiano Viappiani*[,†,||]

Contribution from the Dipartimento di Fisica, Università degli Studi di Parma, Parco Area delle Scienze 7/A, 43100 Parma, Italy, Dipartimento di Biochimica e Biologia Molecolare, Università degli Studi di Parma, Parco Area delle Scienze 23/A, 43100 Parma, Italy, Dipartimento di Sanità Pubblica, Università degli Studi di Parma, via Volturno 39, 43100 Parma, Italy, and CNR-INFM, Parco Area delle Scienze 7/A, 43100 Parma, Italy

Received September 5, 2005; E-mail: cristiano.viappiani@fis.unipr.it

Abstract: Biphasic geminate rebinding of CO to myoglobin upon flash photolysis has been associated to ligand distribution in hydrophobic cavities, structurally detected by time-resolved crystallography, xenon occupancy, and molecular simulations. We show that the time course of CO rebinding to human hemoglobin also exhibits a biphasic geminate rebinding when the protein is entrapped in wet nanoporous silica gel. A simple branched kinetic scheme, involving the bound state A, the primary docking site C, and a secondary binding site B was used to calculate the microscopic rates and the time-dependent population of the intermediate species. The activation enthalpies of the associated transitions were determined in the absence and presence of 80% glycerol. Potential hydrophobic docking cavities within the α and β chains of hemoglobin were identified by computational modeling using xenon as a probe. A hydrophobic pocket on the distal side of the heme, corresponding to Xe4 in Mb, and a nearby site that does not have a correspondence in Mb were detected. Neither potential xenon sites on the proximal side nor a migration channel from the distal to proximal site was located. The small enthalpic barriers between states B and C are in very good agreement with the location of the xenon sites on the distal side. Furthermore, the connection between the two xenon sites is relatively open, explaining why the decreased mobility of the protein with viscosity only slightly perturbs the energetics of ligand migration between the two sites.

Introduction

The role and relevance of cavities in determining functional properties of proteins are becoming progressively established. Cavities lower protein stability, thus favoring flexibility and function-related protein dynamics, and provide routes for ligand entrance to the active site and transient storage.[1] This scenario has many examples in enzyme catalysis where substrate access to and product exit from the active sites occur through well-defined pathways.[2] It is also firmly established for myoglobin (Mb), for which an impressive number of experimental investigations have demonstrated that the migration of carbon monoxide (CO) within the protein matrix involves several hydrophobic pockets. These pockets were first evidenced by X-ray crystallography under xenon high pressure[3] and, more recently, by low temperature[4] and time-resolved X-ray crystallographic studies carried out upon CO flash photolysis.[5−7] The photodissociated CO was located in the Xe1 and Xe4 pockets. Further suggestions about the role of the Xe cavities in ligand migration inside Mb came from computational modeling[8] and molecular dynamics simulations.[9−11] These findings nicely account for CO rebinding kinetics recorded for different Mb mutants.[12,13]

The finding of hydrophobic cavities in several globins, including myoglobin,[12] cytoglobin,[14] neuroglobin,[15] truncated

[†] Dipartimento di Fisica, Università degli Studi di Parma.
[‡] Dipartimento di Biochimica e Biologia Molecolare, Università degli Studi di Parma.
[§] Dipartimento di Sanità Pubblica, Università degli Studi di Parma.
[||] CNR-INFM.

(1) Brunori, M.; Gibson, Q. H. *EMBO Rep.* **2001**, *2*, 674−679.
(2) Prangé, T.; Schiltz, M.; Pernot, L.; Colloc'h, N.; Longhi, S.; Bourguet, W.; Fourme, R. *Proteins: Struct., Funct., Genet.* **1998**, *30*, 61−73.
(3) Tilton, R. F. J.; Kuntz, I. D. J.; Petsko, G. A. *Biochemistry* **1984**, *23*, 2849−2857.
(4) Ostermann, A.; Washipky, R.; Parak, F. G.; Nienhaus, G. U. *Nature* **2000**, *404*, 205−208.
(5) Srajer, V.; Ren, Z.; Teng, T. Y.; Schmidt, M.; Ursby, T.; Bourgeois, D.; Pradervand, C.; Schildkamp, W.; Wulff, M.; Moffat, K. *Biochemistry* **2001**, *40*, 13802−13815.
(6) Bourgeois, D.; Vallone, B.; Schotte, F.; Arcovito, A.; Miele, A. E.; Sciara, G.; Wulff, M.; Anfinrud, P.; Brunori, M. *Proc. Natl. Acad. Sci. U.S.A.* **2003**, *100*, 8704−8709.
(7) Schotte, F.; Lim, M.; Jackson, T. A.; Smirnov, A. V.; Soman, J.; Olson, J. S.; Phillips, G. N., Jr.; Wulff, M.; Anfinrud, P. A. *Science* **2003**, *300*, 1944−1947.
(8) Teeter, M. M. *Protein Sci.* **2004**, *13*, 313−318.
(9) Hummer, G.; Schotte, F.; Anfinrud, P. A. *Proc. Natl. Acad. Sci. U.S.A.* **2004**, *101*, 15330−15334.
(10) Bossa, C.; Anselmi, M.; Roccatano, D.; Amadei, A.; Vallone, B.; Brunori, M.; Nola, A. D. *Biophys. J.* **2004**, 3855−3862.
(11) Bossa, C.; Amadei, A.; Daidone, I.; Anselmi, M.; Vallone, B.; Brunori, M.; Nola, A. D. *Biophys. J.* **2005**, *89*, 465−474.
(12) Scott, E. E.; Gibson, Q. H. *Biochemistry* **1997**, *36*, 11909−11917.
(13) Tetreau, C.; Blouquit, Y.; Novikov, E.; Quiniou, E.; Lavalette, D. *Biophys. J.* **2004**, *86*, 435−447.
(14) deSanctis, D.; Dewilde, S.; Pesce, A.; Moens, L.; Ascenzi, P.; Hankeln, T.; Burmester, T.; Bolognesi, M. *Biochem. Biophys. Res. Commun.* **2004**, *316*, 1217−1221.

hemoglobins (*Paramecium caudatum*, *Chlamydomonas eugametos*, and *Mycobacterium tuberculosis*),[16,17] and *Cerebratulus lacteus* mini-hemoglobin[18] suggests that human hemoglobin (Hb) may also host such cavities. Perhaps surprisingly, a detailed understanding of the internal pathways for CO migration in Hb is not yet available because of limited structural data. A mid-1960s report on Xe binding to horse Hb identified a single external site, possibly due to the low Xe pressure used in that investigation,[19] in agreement with equilibrium binding studies consistent with a single association constant for Xe−Hb complex[20] and the single kinetically resolved binding, later detected by Tilton and Kuntz.[21] More recently, Shibayama and co-workers reported that photodissociated CO molecules in the β subunits of T-state Hb are located at two sites: a distal pocket primary docking site and a hydrophobic cavity in the back of the distal pocket at ∼8.5 Å from the iron.[22] No evidence for this second CO location was reported for T-state α subunits or R-state Hb. However, the low temperature (25−35 K) and dynamic constraints induced by crystal lattice might prevent migration of the ligand, as previously observed for Mb.[4]

We have recently shown that the geminate CO rebinding after flash photolysis of HbCO complexes, entrapped in wet silica gels in the presence of glycerol, is biphasic.[23] CO rebinding kinetics to Hb silica gels is greatly simplified by the absence of overlapping quaternary transitions.[24−26] Biphasic geminate rebinding to both α and β subunits has also been observed in oxygenation studies of tri-liganded R-state Hb.[27] We proposed that these multiple geminate phases might be the evidence for the existence of discrete docking sites for the photodissociated ligand inside the protein matrix. Our model, in analogy with that proposed for Mb[1] to account for the observed rebinding kinetics, is based on a simplified branched four-state model. In this model it is assumed that, after photolysis, the ligand can rebind to the heme from fast rebinding sites, likely present within the distal pocket, or from slower rebinding sites, located farther in the protein matrix. Escape of the ligand to solvent occurs mainly from the distal pocket, as observed for Mb.[1,28]

The differential equations corresponding to Scheme 1 can be solved analytically, and under the hypothesis of preequilibrium for the rebinding from solution, microscopic rates can be obtained. Their values were then calculated from the observed rates, determined from the experimental rebinding curves using a maximum entropy method (MEM).[29,30]

Scheme 1. Simplified Four-State Kinetic Model

$$A(HbCO) \underset{k_{CA}}{\overset{h\nu}{\rightleftharpoons}} C(Hb:CO) \underset{k_{SC}}{\overset{k_{CS}}{\rightleftharpoons}} S(Hb+CO)$$
$$k_{BC} \uparrow\downarrow k_{CB}$$
$$B(Hb::CO)$$

In this work we show that the time course of CO rebinding to Hb can be fairly accurately reproduced with the simple kinetic model of Scheme 1, where structural relaxation and kinetic heterogeneity are neglected. Computational modeling was exploited to identify hydrophobic pockets within both α and β subunits and potential internal pathways for CO migration, with locations compatible with ligand binding kinetics.

Materials and Methods

Computational Modeling. Molecular modeling was carried out on a Silicon Graphics Fuel workstation. The structures of Mb complexed with four Xe atoms (PDB code 1J52) and Hb in the oxygenated state (1HHO),[31] determined at a resolution of 1.9 and 2.1 Å, respectively, were retrieved from the Protein Data Bank (www.rcsb.org). After being imported in the program Sybyl version 7.0 (www.tripos.com), protein structures were carefully checked for atom and bond type correctness assignment. Hydrogen atoms were computationally added using the Sybyl Biopolymer and Build/Edit menus. To avoid negative acid/acid interactions and repulsive steric clashes, added hydrogen atoms were energy minimized with the Powell algorithm with a convergence gradient of 0.5 kcal (mol Å)$^{-1}$ for 1500 cycles. This procedure does not change positions to heavy atoms.

The prediction of Xe atom location was carried out with the computational modeling program GRID, version 22a (www.moldiscovery.com). Using a defined atomic or multiatomic probe, GRID is able to properly locate the energetically and sterically favorable areas in which the probe could be placed.[32] In this study GRID simulations were carried out choosing the Xe atom as the inquiring probe. To properly inspect all the internal protein cavities, a box with dimensions $15 \times 15 \times 15$ Å^3 was centered on Leu72 CG for Mb, Leu66 CD2 for α chains, and Phe71 for β chains of Hb. The grid spacing was set to 0.33 Å. To display cavities and channels connecting different Xe binding sites, Connolly surfaces were built for both Mb and Hb, using the Sybyl MOLCAD module. The measurement of the cavity depth was calculated by building, over the first molecular surface, a second surface with a 6.0 Å radius probe unable to explore smaller cavities. The distance between these two general surface maps is a direct measure of the cavity depth.[33]

Encapsulation of R-State HbCO. A solution containing 10 mM HEPES, 1 mM EDTA, pH 6, was added to an equal volume of tetramethyl orthosilicate (TMOS) and vortexed for 2 min, at 4 °C. The mixture was deoxygenated by bubbling He for 90 min. An equal volume of a solution containing 1% (w/v) human HbA, 10 mM HEPES, 1 mM EDTA, and 30 mM sodium dithionite, pH 6, saturated with CO, was added. The gelation occurred in 10−20 min, at room temperature. When the gel was formed, a solution containing 100 mM HEPES, 1 mM EDTA, and 30 mM sodium dithionite, pH 7, saturated with CO, was layered on it. The sample thickness was approximately 1 mm. Bathing solutions with glycerol concentrations of 0% and 80% (by weight) were used. Samples were stored at 5 °C for 3 days before performing the kinetic experiments to allow for equilibration of the system with CO in the gas phase. Samples were kept at all stages in gastight vials to

(15) Ascenzi, P.; Bocedi, A.; deSanctis, D.; Pesce, A.; Bolognesi, M.; Marden, M. C.; Dewilde, S.; Moens, L.; Hankeln, T.; Burmester, T. *Biochem. Mol. Biol. Educ.* **2004**, *32*, 305−313.
(16) Milani, M.; Pesce, A.; Ouellet, Y.; Ascenzi, P.; Guertin, M.; Bolognesi, M. *EMBO J.* **2001**, *20*, 3902−3909.
(17) Pesce, A.; Couture, M.; Dewilde, S.; Guertin, M.; Yamauchi, K.; Ascenzi, P.; Moens, L.; Bolognesi, M. *EMBO J.* **2001**, *19*, 2424−2434.
(18) Pesce, A.; Nardini, M.; Ascenzi, P.; Geuens, E.; Dewilde, S.; Moens, L.; Bolognesi, M.; Riggs, A. F.; Hale, A.; Deng, P.; Nienhaus, G. U.; Olson, J. S.; Nienhaus, K. *J. Biol. Chem.* **2004**, *279*, 33662−33672,.
(19) Schoenborn, B. P. *Nature* **1965**, *208*, 760−762.
(20) Conn, H. L. J. *J. Appl. Physiol.* **1961**, *16*, 1065−1070.
(21) Tilton, R. F. J.; Kuntz, I. D. J. *Biochemistry* **1982**, *21*, 6850−6857.
(22) Adachi, S.; Park, S. Y.; Tame, J. R. H.; Shiro, Y.; Shibayama, N. *Proc. Natl. Acad. Sci. U.S.A.* **2003**, *100*, 7039−7044.
(23) Sottini, S.; Abbruzzetti, S.; Viappiani, C.; Bettati, S.; Ronda, L.; Mozzarelli, A. *J. Phys. Chem. B* **2005**, *109*, 11411−11413.
(24) Shibayama, N.; Saigo, S. *J. Mol. Biol.* **1995**, *251*, 203−209.
(25) Khan, I.; Shannon, C. F.; Dantsker, D.; Friedman, A. J.; Perez-Gonzales-de-Apodaca, J.; Friedman, J. M. *Biochemistry* **2000**, *39*, 16099−16109.
(26) Abbruzzetti, S.; Viappiani, C.; Bruno, S.; Bettati, S.; Bonaccio, M.; Mozzarelli, A. *J. Nanosci. Nanotechnol.* **2001**, *1*, 407−415.
(27) Lepeshkevich, S. V.; Karpiuk, J.; Sazanovich, I. V.; Dzhagarov, B. M. *Biochemistry* **2004**, *43*, 1675−1684.
(28) Agmon, N. *Biophys. J.* **2004**, *87*, 1537−1543.
(29) Steinbach, P. J.; Ionescu, R.; Matthews, C. R. *Biophys. J.* **2002**, *82*, 2244−2255.
(30) Steinbach, P. J. *J. Chem. Inf. Comput. Sci.* **2002**, *42*, 1476−1478.
(31) Shaanan, B. *J. Mol. Biol.* **1983**, *171*, 31−59.
(32) Goodford, P. J. *J. Med. Chem.* **1985**, *28*, 849−857.
(33) Keil, M.; Exner, T. E.; Brickmann, J. *J. Comput. Chem.* **2003**, *25*, 779−789.

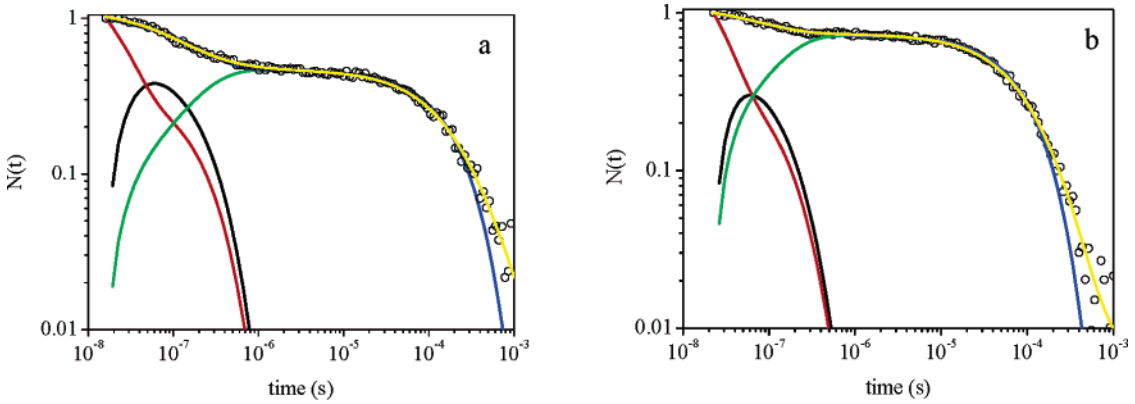

Figure 1. Fitting of the numerical solution of the differential equations (blues curves) derived from Scheme 1 to CO rebinding curves (○) for HbCO gels at 10 (panel a) and 30 °C (panel b). The time courses of the different species are also displayed: $C(t)$, red; $B(t)$, black; $S(t)$, green. The yellow curve is the result of the fit with the MEM analysis.[23]

prevent O_2 leakage into the sample compartment. Absorbance spectra were routinely measured to ensure that HbCO complex was fully formed.[26,34]

Photolysis Setup. The sample was held in a 1 × 1 cm^2 gastight cuvette mounted in a homemade sample holder. The bathing solution was in equilibrium with a 1 atm CO atmosphere. Temperature was controlled by a Peltier element with a feedback control mounted below the cuvette holder. This allowed to achieve temperature stability better than 0.1 °C in the investigated temperature range (10−50 °C). Dry gas flowing on the sample holder prevented condensation of humidity on the cuvette walls. In the flash photolysis setup, photoexcitation was achieved using the second harmonic (532 nm) of a nanosecond Q-switched Nd:YAG laser (Handy Yag HYL-101, Quanta System). Transient absorbance was monitored using a multiline, cw Argon ion laser (2013, Uniphase). The 488 nm line was selected by a Pellin Broca prism and an iris diaphragm. The power on the sample never exceeded 10 mW. Pump and probe beams hit the sample from the same side, approximately at a right angle to the gel surface. The pump beam hit a relatively large sample area (7 mm diameter), containing the spot illuminated by the probe beam (1 mm diameter). Part of the excitation laser output was directed to an energy meter (Laser precision RJ-7620) equipped with a pyroelectric energy probe (Laser precision RJP-735). Experiments were conducted with laser pulse energies of approximately 5 mJ. This energy corresponds to the photolysis of ∼30% of the CO-hemes, resulting in deoxy-heme concentrations of about 100 μM at the end of the laser pulse. To minimize undesired photolysis of samples due to the intense probe beam, a fast mechanical shutter (Uniblitz) was used. The synchronization of the experiment (laser triggering and shutter opening) was performed using home-built electronics.[35] The probe beam was passed through a pinhole and a monochromator (Jobin Yvon H10 UV) for removing the stray light from the pump laser. The intensity of the transmitted light was measured by a Si avalanche photodiode (Hamamatsu S2382), coupled with a transimpedance amplifier (Avtech AV149). The voltage output was recorded by a digital sampling oscilloscope (Lecroy LT374). Typically 100 traces were averaged to yield a transient absorbance signal. Three time scales were used, 1 μs div^{-1}, 100 μs div^{-1}, 1 ms div^{-1}, and 10 000 points were acquired for each trace.

Data Analysis. Numerical solutions to the set of coupled differential equations corresponding to Scheme 1 were determined by using the function ODE15s within Matlab 6.1 (The MathWorks, Inc.). The numerical solution of the set of equations depends on rate constants and concentrations which were considered as fitting parameters that can be optimized using a nonlinear fitting algorithm. For this we used a Matlab version of the optimization package Minuit (CERN).

Results and Discussion

Time Course of CO Rebinding to R-State Hb Gels. The geminate rebinding of CO to Hb in solution has been treated as a first-order rate process, characterized by multiple exponential decays,[36−39] reflecting structural relaxation of the protein.[39−41] This complex situation has been described sometimes with stretched exponential functions.[39,42,43] In the case of Mb, relaxation has been treated explicitly in the framework of ligand migration in the presence of internal docking sites.[28,44] So far, for Hb no attempt has been made to merge the relaxation effects with the presence of distinct docking sites (see below) to describe the rebinding kinetics.

CO rebinding to R-state Hb gels (Figure 1) is characterized by a fast geminate phase and a slower bimolecular phase. The process is simplified with respect to solution because the R to T quaternary transition is significantly slowed,[24,43,45,46] and thus, no CO binding to the T-state is observed. The experimental data can be reproduced fairly well under all investigated conditions (temperature and glycerol concentration) by varying the microscopic rates of the numerical solution of the set of differential equations corresponding to Scheme 1. Figures 1 and 2 show the results of the analysis for selected conditions, demonstrating the general good agreement between the model and the experimental data.

(34) Bruno, S.; Bonaccio, M.; Bettati, S.; Rivetti, C.; Viappiani, C.; Abbruzzetti, S.; Mozzarelli, A. *Protein Sci.* **2001**, *10*, 2401−2407.
(35) Banderini, A.; Sottini, S.; Viappiani, C. *Rev. Sci. Instrum.* **2004**, *75*, 2257−2261.
(36) Jones, C. M.; Ansari, A.; Henry, E. R.; Christoph, G. W.; Hofrichter, J.; Eaton, W. A. *Biochemistry* **1992**, *31*, 6692−6702.
(37) Goldbeck, R. A.; Paquette, S. J.; Björling, S. C.; Kliger, D. S. *Biochemistry* **1996**, *35*, 8628−8639.
(38) Esquerra, R. M.; Goldbeck, R. A.; Reaney, S. H.; Batchelder, A. M.; Wen, Y.; Lewis, J. W.; Kliger, D. S. *Biophys. J.* **2000**, *78*, 3227−3239.
(39) Henry, E. R.; Jones, C. M.; Hofrichter, J.; Eaton, W. A. *Biochemistry* **1997**, *36*, 6511−6528.
(40) Lyons, K. B.; Friedman, J. M. In *Hemoglobin and oxygen binding*; Ho, C., Eaton, W. A., Collman, J. P., Gibson, Q. H., Leigh, J. S., Margolias, E., Moffat, K., Scheidt, W. R., Eds.; Elsevier/North-Holland: Amsterdam, 1982.
(41) Frauenfelder, H.; Nienhaus, G. U.; Johnson, J. B. *Phys. Chem. Chem. Phys.* **1991**, *95*, 272−278.
(42) Sottini, S.; Viappiani, C.; Ronda, L.; Bettati, S.; Mozzarelli, A. *J. Phys. Chem. B* **2004**, *108*, 8475−8484.
(43) Viappiani, C.; Bettati, S.; Bruno, S.; Ronda, L.; Abbruzzetti, S.; Mozzarelli, A.; Eaton, A. W. *Proc. Natl. Acad. Sci. U.S.A.* **2004**, *101*, 14414−14419.
(44) Dantsker, D.; Samuni, U.; Friedman, J. M.; Agmon, N. *Biochim. Biophys. Acta* **2005**, *1749*, 234−251.
(45) Bettati, S.; Mozzarelli, A. *J. Biol. Chem.* **1997**, *272*, 32050−32055.
(46) Das, T. K.; Khan, I.; Rousseau, D.; Friedman, J. M. *Biospectroscopy* **1999**, *5*, S64−S70.

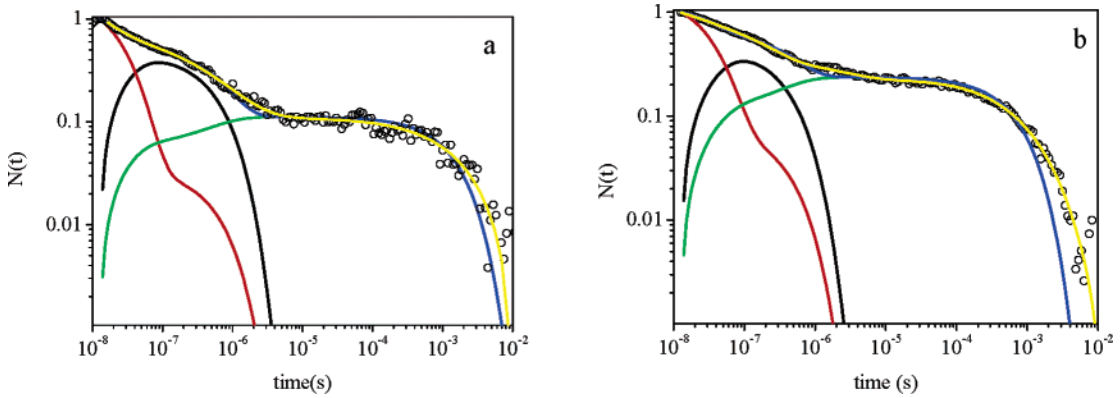

Figure 2. Fitting of the numerical solution of the differential equations (blue curves) derived from Scheme 1 to CO rebinding curves (○) for HbCO gels in 80% glycerol at 10 (panel a) and 30 °C (panel b). The time course for the different species is also displayed: $C(t)$, red; $B(t)$, black; $S(t)$, green. The yellow curve is the result of the fit with the MEM analysis.[23]

Table 1. Rate Constants at 20 °C and Activation Enthalpies in the Absence and Presence of 80% Glycerol

	C→A	B→C	C→B	C→S	S→C
			no glycerol		
k (10^6 s^{-1})	6.4	19.7	26.2	9.7	20 M^{-1}
E_a (kcal/mol)	0	1.8 ± 0.6	0	7.6 ± 0.5	16 ± 1
			80% glycerol		
k (10^6 s^{-1})	21.4	3.7	26.7	3.2	3.1 M^{-1}
E_a (kcal/mol)	0	4.0 ± 0.5	0	4.4 ± 0.8	8.3 ± 0.4

After photolysis, CO present in state C disappears with a rate that is temperature and glycerol dependent, partly populating state B and partly escaping to solution, state S. This can be appreciated in the rising phase of the curve describing state S, in which two separate rates can be distinguished, the faster being due to direct escape of photodissociated ligand from state C and the slower to those ligand molecules that are escaping to solvent coming from state B. The extent to which state B is populated depends on glycerol and temperature. Table 1 reports the microscopic rate constants at 20 °C for the four state model. The linear Arrhenius plots obtained from the rate constants in the temperature range 10−50 °C (Supplementary Information) allowed us to estimate the activation enthalpies reported in Table 1. Under all conditions, the fitting obtained with the MEM is superior to the fit obtained with the numerical solution of the differential equations. This is particularly true for the long time tail of the bimolecular rebinding and for the transition between the geminate and the bimolecular phase (Figures 1 and 2, yellow curves).[23] This is mainly due to the simplified kinetic model which uses single rates to describe the observed kinetics. The MEM retrieves lifetime distributions which can give a better description of kinetic heterogeneity due to kinetic hole burning and structural relaxation accompanying ligand rebinding.[23] As a consequence, the recovered rates and the activation enthalpies (Table 1) are also slightly different for the two analyses, although the overall picture is substantially the same.

Although simplified, the present analysis allows us to reproduce the population of the state B also in the absence of glycerol. This state is populated to a lower extent with respect to samples containing glycerol. Nevertheless, its time course is clearly retrievable from the experimental traces, demonstrating that the population of the state B is detectable also at lower viscosity.

The rates and the activation enthalpies reported in Table 1 for the glycerol containing samples are not substantially different from those obtained with the MEM.[23] At variance, some of the microscopic rates obtained from the present analysis of the CO rebinding kinetics to the glycerol free samples differ considerably from the previous estimate.

The rates k_{CA} and k_{CB} are characterized by negligible activation enthalpies, independently of glycerol content. The activation enthalpy for the rate k_{BC} is of the order of 2 kcal/mol in water and is slightly increased (4.0 kcal/mol) in 80% glycerol. Modest effects are also observed on the activation enthalpy that CO must overcome to escape to solvent (rate k_{CS}). The present analysis confirms the finding that, while the activation enthalpy for process C→A is not influenced by the presence of glycerol, the rate k_{CA} for returning to state A is dramatically increased. This explains the higher geminate yield in 80% glycerol, despite the decreased activation enthalpy for process C→S.

The lack of effects of viscosity on the rate k_{CB} indicates that no large protein fluctuations are required to open pathways for ligand migration from site C to site B. The rate k_{BC}, on the other hand, is reduced 5-fold in 80% glycerol. Thus, contrary to what we observed previously,[23] the process B→C seems to be hindered, rather than favored, by the increased viscosity. Thus, the higher efficiency with which state B is populated in 80% glycerol arises from a decrease in the escape rate from state B (k_{BC}).

The activation enthalpy for the S→C and C→S processes are reduced in the presence of 80% glycerol. We have previously discussed this effect as due to the opposing effects of increasing the concentration of cosolutes (glycerol) which, at the same time, affects the activity of the reactants, the solubility of CO, and the viscosity of the medium.[42]

Locations of Cavities in α and β Subunits of Hb by Computational Modeling. Hydrophobic cavities both for Mb and Hb were localized by exploring the protein matrix using the software GRID[32] and a Xe atom as probe. The search procedure, applied to Mb, correctly identified the Xe1, X3, and Xe4 sites (Figure 3) that were crystallographically detected.[3] The same analysis, applied to the α and β chains of R-state Hb, shows very interesting results (Figure 4). There are two well-defined potential Xe binding sites. The larger one corresponds to the Xe4 position, whereas the second, smaller contour does not have a correspondence in Mb. This can be due to amino acid substitutions that might change cavity volume: Leu135 ⇒ βVal134, Met131 ⇒ βTyr130. The Xe1 cavity of Mb on

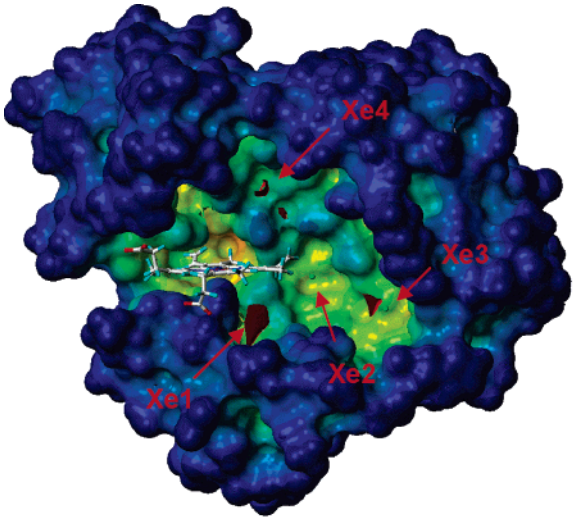

Figure 3. Connolly surface of Mb crystallized in the presence of Xe (1J52), built with Sybyl MOLCAD tools. External protruding regions are colored blue, while cavities and clefts are colored green, yellow, and orange, as a function of depth. The amino acids forming part of the external surface have been removed to display the positions occupied by the four Xe atoms (Xe1, Xe2, Xe3, and Xe4), crystallographically detected (green spheres) and localized by red arrows. The red contours identify the energetically and sterically favorable regions for Xe sites, detected by GRID. The Xe1 and Xe4 atoms are completely hidden by the contour.

the proximal side, where CO was also crystallographically observed, was not present in the α nor in the β chains of Hb.

Moreover, several mutations of β-chain Hb in the region homologous to Mb Xe1 site would apparently prevent Xe migration from Xe4 site to Xe1. The more significant and obstructing substitutions are as follows: Phe138 ⟹ βVal137, Leu86 ⟹ βPhe85, and, in particular, Leu104 ⟹ βPhe103 and Ile142 ⟹ βLeu141. Accordingly, the Leu104Trp mutation in Mb caused a significant decrease in the occupancy of the proximal site.[12] Moreover, the side chains of the substituted amino acids extensively occupy the Xe1 site in the β subunit, making it unsuitable for Xe accommodation. Analogous considerations can hold for the α chain of Hb, where the corresponding mutations are Leu104 ⟹ αPhe98 and Ile142 ⟹ αLeu136. Also in the α chain the Xe1 site is not identified by GRID as a potential binding site for Xe. Other mutations occur in the Xe2 and Xe3 sites, which are less accessible in both α and β Hb chains with respect to Mb (the more significant mutations are highlighted in bold): Xe2 binding pocket − Leu104 ⟹ αPhe98, Ser108 ⟹ αSer102, Leu135 ⟹ αLeu129, Phe138 ⟹ αVal132, **Arg139** ⟹ α**Ser133** in the α chain, and Leu104 ⟹ βPhe103, Ser108 ⟹ βGly107, Leu135 ⟹ βVal134, Phe138 ⟹ βVal137, Arg139 ⟹ βAla138 in the β chain; Xe3 binding pocket − Trp7 ⟹ αLeu2, **His82** ⟹ α**Met76**, Ala134 ⟹ αPhe138, Leu137 ⟹ αSer131, Phe138 ⟹ αVal132 in the α chain, and Trp7 ⟹ βLeu78, Ile75 ⟹ βGly74, **His82** ⟹ β**Leu81**, Leu137 ⟹ βGly136 in the β chain.

CO Binding and Migration. Recent crystallographic studies have identified the CO location, upon photodissociation, in both the R and T states of Hb.[22] In T-state β subunits, photodissociated CO molecules are detected at two different binding sites, placed respectively 3.7 Å and 8.5 Å apart from the heme iron. The first site, in the distal heme pocket above pyrrole ring C, corresponds to the primary docking site of photolyzed CO in Mb.[5,47−49] The second site remarkably coincides with the larger Xe contour that we have identified by GRID (Figures 3 and 4) and corresponds to the Xe4 pocket of Mb. This cavity is surrounded by the hydrophobic residues Gly24, Ala27, Leu28, Val67, Leu68, and Leu106. In the α chain, CO has not been detected in this pocket but only in a location at about 3.5 Å from the iron. This different behavior of the α subunit can be attributed to several mutations occurring in the cavity, as described above, and also to the different location of Leu110 side chain, which seems to control the communication between the possible Xe sites identified by GRID in the α and β chain (Figure 5). The hydrophobic side chain of Leu68, and the different location of the Leu110 side chain probably make the connection between the two areas more difficult in the β with respect to the α subunit. No secondary binding sites have been reported in the R state by Adachi and co-workers,[22] possibly due to the low temperature (35 K), preventing migration of the ligand, as previously observed for Mb.[4]

The channel connecting the heme iron binding site to the exterior is very similar in Mb and Hb. No significant mutations are observed, except Thr67 ⟹ αLys61 and the corresponding

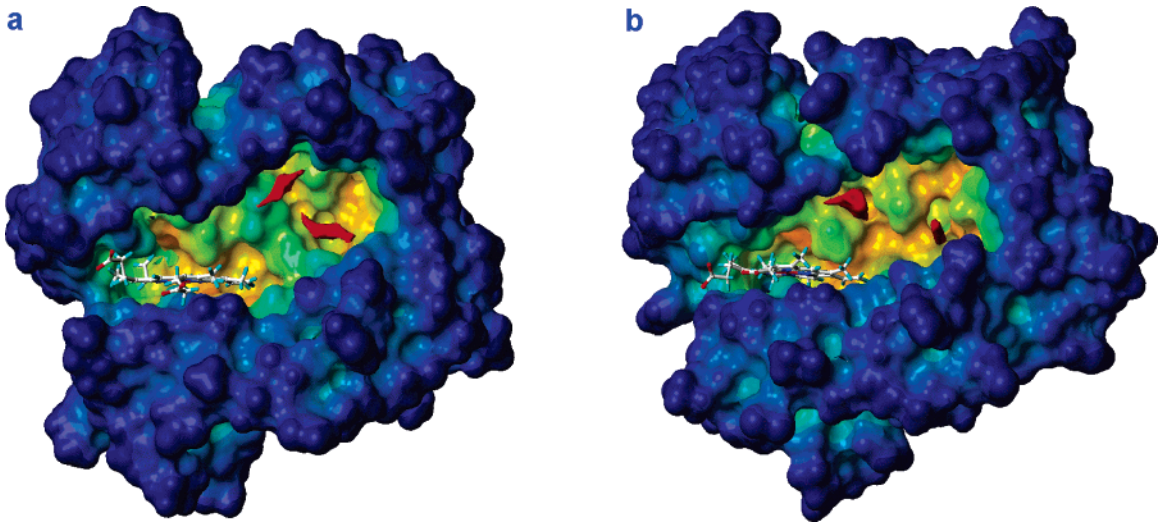

Figure 4. Connolly surface of α (panel a) and β (panel b) chains of oxyHb (1HHO), built with Sybyl MOLCAD tools. The red GRID contours identify regions energetically and sterically available to be occupied by Xe atoms. Part of the external amino acids have been removed to clearly display the cavities and the channel connecting the heme and the two Xe sites.

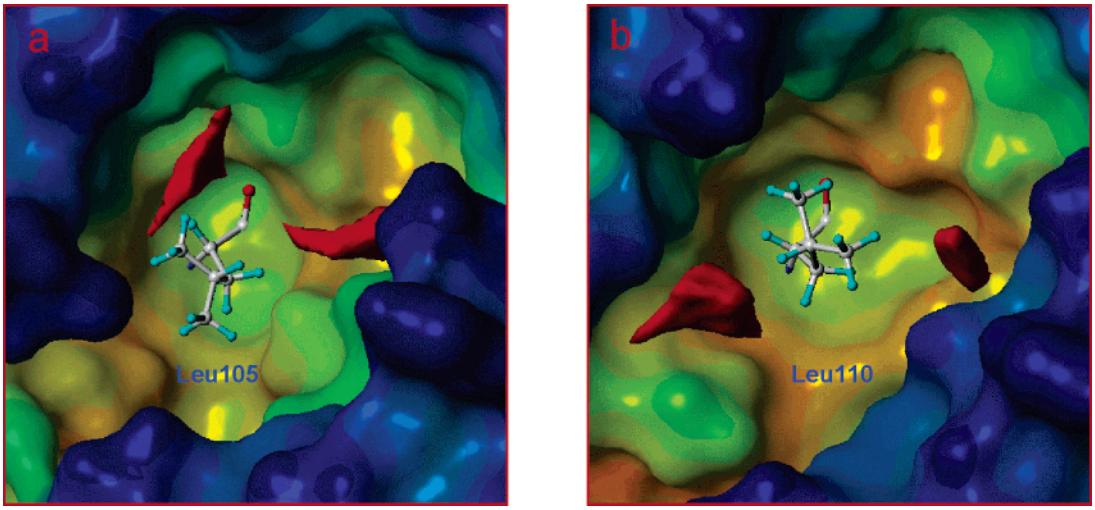

Figure 5. Close-up view of predicted Xe sites. (a) GRID contours identify the probable Xe sites in oxyHb α subunits. (b) GRID contours identify the probable Xe sites in oxy-Hb β subunits. The communication between the two sites is controlled by the side chain of Leu105 in the α chain and Leu110 in the β chain. The different contour shape is due to mutations occurring in the internal cavities: αAla63 ⇒ βLeu68 and αTyr24 ⇒ βVal23.

Thr67 ⇒ βLys66. The Lys side chain is effectively more obstructive than Thr but is also extremely mobile, as evidenced by high B factors. Therefore, the pathway followed by CO to leave the protein matrix and exit to the solvent might be similar.

The meaning of the microscopic rates and the enthalpic barriers can be discussed in light of the computational modeling results. The finding of small activation enthalpies between states B and C from the ligand rebinding kinetics is in very good agreement with the location of the Xe sites on the distal side, which could potentially act as docking sites also for the photodissociated CO. While the connection between the two Xe sites is relatively open, the decreased mobility of the protein when the viscosity is increased seems to slightly increase the enthalpic barrier for process B→C, thus stabilizing the photodissociated ligand in state B. This small increase, coupled with the dramatic drop in the rate for the process B→C when glycerol is added, and the unchanged rate and enthalpic barrier for the reverse (C→B) reaction make state B a very efficient trap for the photodissociated ligand. The reduced mobility of critical residues in the channel connecting the two Xe sites (e.g., β Leu105 and α Leu110, Figure 5) may limit the B→C rate. A slower redistribution of conformational substates could also contribute to the observed reduction in k_{BC}, in agreement with the broader lifetime distributions observed for HbCO gels in the presence of 80% glycerol.[23] This effect also could be at the basis of the increased rate of the process C→A.

However, the influence of glycerol on k_{CS} suggests that the reduced mobility of the protein, due to the increased viscosity, decreases the rebinding rate even in the presence of a decreased enthalpic barrier, possibly due to the opposing effect of the lower CO solubility. The effect of glycerol on k_{SC} is similar, with the reduction in rate being more substantial. The above-mentioned substitutions Thr67 ⇒ αLys61 and Thr67 ⇒ βLys66, with the Lys side chain being more bulky than Thr, could be responsible for the reduction of the rates k_{SC} and k_{CS} at high viscosity. Their mobility could be strongly reduced when glycerol is added, and this would decrease the probability of rebinding.

Conclusions

Encapsulation in wet nanoporous silica gels allows us to simplify the kinetics of CO rebinding to Hb by hampering tertiary and quaternary structural relaxation on the time scale of the experiments. This allowed us to highlight biphasic geminate rebinding to Hb at room temperature, even in the absence of viscogenic agents. The observed kinetics are satisfactorily described by a simple branched four-state kinetic model, and can be associated to ligand distribution in internal hydrophobic cavities as in the case of Mb. In the absence of detailed structural evidence for Hb, computational modeling was used to identify potential CO docking sites within α and β subunits, which are compatible with the observed kinetic behavior and with the effect of glycerol on ligand migration and distribution of intermediate states. A comparison of the CO binding sites and ligand migration pathways retrieved for Hb with those of Mb suggests possibly distinct functional roles of the internal cavities. The present work lays important groundwork for time-resolved crystallography studies on HbCO and calls for kinetic investigation of Hb mutants of the docking sites.

Acknowledgment. The authors acknowledge MIUR (FIRB nanotechnologies, and PRIN2004), CNR (Functional Genomics), CNR-INFM, and 6th European Union Framework Project "Euroblood Substitutes" for financial funding. P. J. Steinbach is kindly acknowledged for the use of MemExp.

Supporting Information Available: Arrhenius plot for the microscopic rate constants. This material is available free of charge via the Internet at http://pubs.acs.org.

JA056101K

(47) Teng, T. Y.; Šrajer, V.; Moffat, K. *Nat. Struct. Biol.* **1994**, *1*, 701−705.
(48) Schlichting, I.; Berendzen, J.; Phillips, G. N.; Sweet, R. M. *Nature* **1994**, *371*, 808−812.
(49) Hartmann, H.; Zinser, S.; Komninos, P.; Schneider, R. T.; Nienhaus, G. U.; Parak, F. *Proc. Natl. Acad. Sci. U.S.A.* **1996**, *93*, 7013−7016.